



# Stereological study of organelle distribution in human oocytes at metaphase I

Sofia Coelho<sup>1,2,\*</sup> , Ana Sílvia Pires-Luís<sup>3,4,\*</sup>, Elsa Oliveira<sup>1,5</sup>, Ângela Alves<sup>1,5</sup>, Carla Leal<sup>6</sup>, Mariana Cunha<sup>7</sup>, Márcia Barreiro<sup>6</sup>, Alberto Barros<sup>7,8,9</sup>, Rosália Sá<sup>1,5</sup> and Mário Sousa<sup>1,5</sup> 

## Research Article

**Cite this article:** Coelho S *et al.* (2020) Stereological study of organelle distribution in human oocytes at metaphase I. *Zygote*. **28**: 308–317. doi: [10.1017/S0967199420000131](https://doi.org/10.1017/S0967199420000131)

Received: 26 December 2019  
Accepted: 17 February 2020  
First published online: 14 April 2020

### Keywords:

Human immature oocytes; Human metaphase I oocytes; Human oocytes; Stereology; Ultrastructure

### Author for correspondence:

Mário Sousa. Laboratory of Cell Biology, Department of Microscopy, Institute of Biomedical Sciences Abel Salazar (ICBAS), University of Porto (UP), Rua Jorge Viterbo Ferreira, 228, 4050-313 Porto, Portugal. Tel: +351 919974476. E-mail: [msousa@icbas.up.pt](mailto:msousa@icbas.up.pt)

\*Both authors contributed equally to this work.

<sup>1</sup>Laboratory of Cell Biology, Department of Microscopy, Institute of Biomedical Sciences Abel Salazar (ICBAS), University of Porto (UP), Rua Jorge Viterbo Ferreira, 228, 4050-313 Porto, Portugal; <sup>2</sup>Department of Life Sciences, Faculty of Sciences and Technology, New Lisbon University (UNL), Campus da Caparica, 2829-516 Lisbon, Portugal; <sup>3</sup>Laboratory of Histology and Embryology, Department of Microscopy, Institute of Biomedical Sciences Abel Salazar, University of Porto, Rua Jorge Viterbo Ferreira, 228, 4050-313 Porto, Portugal; <sup>4</sup>Department of Pathology, Hospital Centre of Vila Nova de Gaia/Espinho, Unit 1, Rua Conceição Fernandes, 1079, 4434-502 Vila Nova de Gaia, Portugal; <sup>5</sup>Multidisciplinary Unit for Biomedical Research (UMIB), University of Porto, Portugal; <sup>6</sup>Centre of Assisted Medical Procreation (CPMA), Maternal Child Centre of the North (CMIN), Hospital and University Center of Porto (CHUP), Largo da Maternidade de Júlio Dinis, 4050-651 Porto, Portugal; <sup>7</sup>Center for Reproductive Genetics A. Barros (CGR), Av. do Bessa, 240, 1<sup>o</sup> Dto. Frente, 4100-012 Porto, Portugal; <sup>8</sup>Department of Genetics, Faculty of Medicine, University of Porto (FMUP), Alameda Prof. Hernâni Monteiro, 4200-319 Porto, Portugal and <sup>9</sup>Institute of Health Research and Innovation (IPATIMUP/i3S), University of Porto, Rua Alfredo Allen, 208, 4200-135 Porto, Portugal

## Summary

We have previously presented a stereological analysis of organelle distribution in human prophase I oocytes. In the present study, using a similar stereological approach, we quantified the distribution of organelles in human metaphase I (MI) oocytes also retrieved after ovarian stimulation. Five MI oocytes were processed for transmission electron microscopy and a classical manual stereological technique based on point-counting with an adequate stereological grid was used. Kruskal–Wallis and Mann–Whitney *U*-tests with Bonferroni correction were used to compare the means of relative volumes (*V*<sub>v</sub>) occupied by organelles. In all oocyte regions, the most abundant organelles were mitochondria and smooth endoplasmic reticulum (SER) elements. No significant differences were observed in *V*<sub>v</sub> of mitochondria, dictyosomes, lysosomes, or SER small and medium vesicles, tubular aggregates and tubules. Significant differences were observed in other organelle distributions: cortical vesicles presented a higher *V*<sub>v</sub> ( $P = 0.004$ ) in the cortex than in the subcortex (0.96% vs 0.1%) or inner cytoplasm (0.96% vs 0.1%), vesicles with dense granular contents had a higher *V*<sub>v</sub> ( $P = 0.005$ ) in the cortex than in the subcortex (0.1% vs 0%), and SER large vesicles exhibited a higher *V*<sub>v</sub> ( $P = 0.011$ ) in the inner cytoplasm than in the subcortex (0.2% vs 0%). Future stereological analysis of metaphase II oocytes and a combined quantitative data of mature and immature oocytes, will enable a better understanding of oocyte organelle distribution during *in vivo* maturation. Combined with molecular approaches, this may help improve stimulation protocols and *in vitro* maturation methods.

## Introduction

After ovarian-controlled hormonal hyperstimulation in assisted reproductive treatments (ART), most (about 85–90%) of retrieved oocytes are in the mature metaphase II (MII) stage and about 10–15% of oocytes are immature, either in prophase I (GV, germinal vesicle) or metaphase I (MI) (Chian *et al.*, 2013).

Immature oocytes can be tested *in vitro* to evolve to mature oocytes, allowing for ART use by intracytoplasmic sperm injection (ICSI), which could be an advantage in cases of absence or low number of MII oocytes (Nogueira *et al.*, 2009; Smitz *et al.*, 2011). Some immature oocytes may spontaneously reach the final stage of nuclear maturation within 24 h after oocyte retrieval, and these rates may be increased (to about 80%) when immature oocytes are cultured in maturation medium supplemented with gonadotrophins (Cha and Chian, 1998) and growth hormones (Richani and Gilchrist, 2018; Li *et al.*, 2019).

Several reports have shown contradictory results following the use of MI oocytes in ICSI treatments. A case with recurrent retrieval of MI oocytes after ovarian stimulation revealed that those oocytes were devoid of *in vitro* maturation capacity and ultrastructural analysis showed disrupted spindle formation in the presence of a conserved cytoplasm morphology (Windt *et al.*, 2001). A similar report, with recurrent retrieval of MI oocytes after ovarian stimulation, also showed that MI oocytes were unable to mature *in vitro* (Levran *et al.*, 2002). However, other

authors have reported evidence that some MI oocytes could mature *in vitro* into MII oocytes and therefore be used for ICSI treatments. In a study, after microinjection of MI oocytes, authors observed higher degeneration rates, lower fertilization rates and higher rates of multinucleated zygotes compared with MII oocytes, but some attained the embryo cleavage stage. After transfer of these embryos, a successful pregnancy, with the birth of a healthy newborn with a normal karyotype, was achieved (Strassburger *et al.*, 2004). These results were further supported by similar observations, in which some MI oocytes matured *in vitro* in MII oocytes, with these MII oocytes being able to fertilize and lead to successful pregnancies (Strassburger *et al.*, 2004).

The successful use of MI oocytes in ICSI treatments can only be possible if the MI oocyte achieved to correctly expel the second polar body and therefore originate a haploid female pronucleus. However, it is not advisable to use MI oocytes for ICSI treatments, as a parthenogenic activation of the oocyte, elicited by the injection procedure, would lead to the formation of a diploid female pronucleus (absence of second polar body extrusion). In contrast, the use of *in vitro* matured MI oocytes to MII oocytes, is justified when few MII oocytes are available or when all retrieved oocytes are at the MI stage (Vanhoutte *et al.*, 2005; Álvarez *et al.*, 2013). Nevertheless, it is of note that embryos originating from MI oocytes present higher rates of chromosomal aneuploidy, even after *in vitro* maturation to MII oocytes (Strassburger *et al.*, 2010).

Earlier reports described MI oocyte ultrastructure. Some described the ooplasm and metaphase I plate (Zamboni *et al.*, 1972; Sathananthan, 1994; El Shafie *et al.*, 2000; Morimoto, 2009). Others presented the nuclear changes occurring during maturation, from GV to MI and from MI to MII (Sathananthan, 1985; Sathananthan *et al.*, 1986). And others briefly described the ooplasm, with images (Sundström *et al.*, 1985a,b; Motta *et al.*, 1988; Familiari *et al.*, 1989; Sathananthan, 2000, 2003) or without images (Sundström and Nilsson, 1988). From these studies, analysis of MI oocyte ultrastructure revealed a mature appearance of the zona pellucida, a short perivitelline space, numerous narrow and moderately long microvilli, some cortical vesicles beneath the oolemma, numerous oval and elongated mitochondria, some adjacent to smooth endoplasmic reticulum (SER) vesicles, numerous small SER vesicles and tubules, and rare dictyosomes, annulate lamellae, rough endoplasmic reticulum and lysosomes.

To further complement these descriptive data, in the present study we quantified the organelle distribution in MI oocytes using a stereological approach. To our knowledge, this is the first stereological analysis of human MI oocytes. We believe that this kind of analysis complements morphological and molecular studies and helps to better understand the cellular mechanisms underlying oocyte maturation, which may be important for the development of new *in vitro* maturation methods and oocyte quality markers.

## Materials and methods

### Ethical approval

Ethical guidelines were followed conducting the research, with written informed consent obtained before experiments. This work did not involve experiments on humans or animals. Donated surplus immature oocytes were used. The approval of the Ethics Committee and the Helsinki Declaration, revised in Tokyo 2004, on human experimentation does not apply to this work. The procedures of the private infertility clinic CGR and the In Vitro

Fertilization (IVF) unit of the Public Hospital CMIN-CHUP are under provisions of the National Law on Medically Assisted Procreation (Law of 2017) and overseen by the National Council on Medically Assisted Procreation (CNPMA-2018). According to these rules and guidelines, the use of clinical databases and patient biological material for diagnosis and research may be used without additional ethical approval, under strict individual anonymity, and after patient informed and written consent. Regarding the use of immature oocytes for electron microscopy at ICBAS-UP, the Ethics Committee authorization number is Project: 2019/CE/P017 (266/CETI/ICBAS).

### Patients

We performed this research using five MI oocytes retrieved after controlled ovarian stimulation during ART treatments performed at CGR and CMIN-CHUP.

### Ovarian-controlled hyperstimulation

Women underwent controlled ovarian hyperstimulation with a gonadotrophin-releasing hormone (GnRH) antagonist protocol (0.25 mg cetrorelix, Cetrotide; Merck-Serono, London, UK; or 0.25 mg ganirelix, Orgalutran; MSD, Hertfordshire, UK); or with a long agonist protocol (0.1 mg triptorelin, Decapeptyl; Ipsen Pharma Biotech, Signes, France). For stimulation, recombinant follicle stimulating hormone (rFSH, follitropin beta, Puregon; MSD, Haalem, The Netherlands; or rFSH, follitropin alfa, Gonal-F; Merck-Serono) was used alone or in combination with: human menopausal gonadotropin (HMG, Menopur; Ferring, Kiel, Germany) or recombinant luteinizing hormone (rLH lutropin alfa + rFSH follitropin alfa, rLH+rFSH, Pergoveris, Merck-Serono; or rLH, Luveris, Merck-Serono). In some cases, only HMG was used. The ovulation trigger was performed with recombinant choriogonadotropin alpha (rHCG, 250 µg, Ovitrelle; Merck-Serono), with a GnRH agonist (0.2 mg triptorelin), or with a dual trigger, using triptorelin (0.2 mg) and rHCG (250 µg). Serum estradiol testing was on the day of HCG trigger or 1 day before (Huirne *et al.*, 2007; Pinto *et al.*, 2009).

### Gamete and embryo handling

Procedures were performed on a K-Systems laminar flow with thermal base (Cooper Surgical, Malöv, Denmark). For IVF, cumulus-oocyte complexes (COC) were collected in SynVivo Flush medium (without heparin, Origio, Malöv, Denmark). All media were devoid of phenol red. After this step, gamete handling was performed under paraffin oil (Ovoil-100, VitroLife, Frölunda, Sweden). COCs were washed with SynVivo Flush medium in 1-well culture dishes (Falcon, Corning, New York, NY, USA). They were then transferred to an ESCO incubator (MRI-6A10, ESCO Medical, Singapore, Singapore) (37°C, 5% O<sub>2</sub>, 6% CO<sub>2</sub>, 89% N<sub>2</sub>, in a humidified atmosphere) with Sequential Fert (Origio) and incubated for 2 h. Thereafter, they were denuded, for 30 s, with recombinant hyaluronidase (ICSI Cumulase, Origio), washed with sperm preparation medium (SPM) and then mechanically dissociated from granulosa cells in SPM (Origio) with oocyte denudation micropipettes (Vitrolife). Denudation was performed at 37°C (thermal laminar flow base). After denudation, immature oocytes were transferred to SPM-containing tubes (Falcon, Corning) and processed for transmission electron microscopy (TEM).

### Transmission electron microscopy

Oocytes were fixed with Karnovsky (2.5% glutaraldehyde, 4% paraformaldehyde, 0.15 M sodium cacodylate buffer) (Sigma-Aldrich, St. Louis, USA; Merck, Darmstadt, Germany) at room temperature for 30 min followed by 2 h at 4°C. After washing in 0.15 M sodium cacodylate buffer, pH 7.3 (Merck) for 2 h at 4°C, the oocytes were post-fixed with 2% osmium tetroxide (Merck) in buffer containing 0.8% potassium ferricyanide (Merck) for 2 h at 4°C. Oocytes were then washed in buffer (10 min), serially dehydrated in ethanol (Panreac, Barcelona, Spain), equilibrated with propylene oxide (Merck) and embedded in Epon (Sigma). Semithin and ultrathin sections were prepared with a diamond knife (Diatome, Hatfield, Switzerland) on an LKB ultramicrotome (Leika Microsystems, Weltzlar, Germany). Using a Random Number Table for the initial cut, MI oocytes were serially sectioned and the ultrathin sections were collected and analyzed every 15 µm. Ultrathin sections were collected on 100-mesh formvar carbon-coated copper grids (Taab, Berks, UK), stained with 3% aqueous uranyl acetate (20 min) (BDH, Poole, UK) and Reynolds lead citrate (10 min) (Merck). Ultrathin sections were observed under a JEOL 100 CXII transmission electron microscope (JEOL, Tokyo, Japan) operated at 60 kV (Sousa and Tesarik 1994; El Shafie *et al.*, 2000; Sá *et al.*, 2011).

### Stereological and statistical analysis

For each microscope grid, a systematic sampling was performed, with photographs taken at alternate TEM field spaces when more than 50% of the field was occupied by the oocyte cytoplasm. Images were taken at ×5300 magnification and printed at 20.2 cm × 20.2 cm. A classic manual stereological technique based on point-counting with an adequate stereological grid was used (Fig. 1A). Printed photographs were placed under a stereological grid and the number of grid points placed over each organelle was noted (Fig. 1B, C). The relative volume (Vv) of each organelle was obtained by applying the formula  $Vv(\text{organelle, oocyte}) = [\text{number of points (organelle)/number of points (oocyte)}] \times 100$  (%) as previously described (Weibel *et al.*, 1966). All measurements were performed in the printed version. The organelles included in the evaluation were: cortical vesicles (CV), vesicles containing granular material (VZ), mitochondria (Mi), dictyosomes (Di), lysosomes (Ly), SER tubular aggregates (aSERT), SER isolated tubules (SER-IT), SER small vesicles (SER-SV: smaller than mitochondria), SER medium vesicles (SER-MV: about the size of mitochondria), SER large vesicles (SER-LV: larger than mitochondria), and total SER (SV, MV, LV, IT, aSERT).

In addition, each oocyte was divided into three regions from the oolemma up to the cell centre: cortex (5 µm), subcortex (5–10 µm) and inner cytoplasm (>10 µm) (Fig. 2). The same stereological procedure was then adopted, applying the formula  $Vv(\text{organelle, cortex/subcortex/inner cytoplasm}) = [\text{number of points (organelle)/number of points (cortex/subcortex/inner cytoplasm)}] \times 100$  (%) (Pires-Luís *et al.*, 2016).

Statistical analysis was performed with Microsoft Excel 2007 and SPSS version 22.0 (IBM Corp, Foster City, California, CA, USA). Results are presented as mean, standard error of the mean (SEM = standard deviation/ $n^{1/2}$ ) and coefficient of variation (CVar = standard deviation/mean).

Normal distribution was tested with the Kolmogorov–Smirnov test. As the samples did not follow a normal distribution, non-parametric tests were used. Kruskal–Wallis and Mann–Whitney *U*-tests with Bonferroni correction were used to compare the

means of Vv (organelle, oocyte), Vv (organelle, cortex), Vv (organelle, subcortex) and Vv (organelle, inner cytoplasm). Statistical significance level was set at  $P < 0.05$ .

### Results

At the inverted microscope, live MI oocytes (Fig. 1D) appeared as a roundish cell separated from a translucent thick zona pellucida (ZP) by a short and narrow perivitelline space. The ooplasm presented a slight granularity in the inner region.

In semithin sections (Fig. 1E–G), the perivitelline space evidenced remnants of follicular cell feet and oocyte microvilli, with cortical vesicles under the oolemma. The remainder of the ooplasm contained mitochondria and lucent vesicles. A network of areas devoid of major organelles appeared markedly large at the oocyte cortex and subcortex. On one of the cell's poles, near the surface, was the metaphase I plate.

At the ultrastructural level, the oocyte surface evidenced numerous narrow and long microvilli (Fig. 2). Under the oolemma, there was a continuous row of dense CV and coated-vesicles (Figs 2 and S1). Isolated CVs were observed in the subcortex (Fig. 2B) and inner ooplasm (Fig. 3B). The cortical region also contained small vesicles containing granular materials (VZ), which seemed to expel their contents into the perivitelline space (Fig. S1). The remainder ooplasm was filled with SER small (SV), medium (MV) and large (LV) vesicles, SER-IT and mitochondria (Figs 2 and 3). The ooplasm also contained SER tubular aggregates (aSERT) (Fig. S2B, C), lysosomes (Fig. S2D, E), and small dictyosomes (Fig. S3). The Metaphase I plate was observed traversing the three regions of the oocyte, without centrioles at the chromosome poles (Fig. S2A). We did not observe annulate lamellae, rough endoplasmic reticulum cisternae, multivesicular bodies, lipid droplets or polyribosomes. As we did not perform cytochemical analyses, it was not possible to exclude the presence of primary lysosomes or peroxisomes.

The present stereological analysis was performed on 320 photographs, 153 with representation of the oocyte cortex, 142 with representation of the oocyte subcortex and 167 with representation of the oocyte inner cytoplasm (Figs 2 and 3). Quantified organelles were cortical vesicles, VZ vesicles, mitochondria, lysosomes, dictyosomes, aSERT, SER-IT and SER small, medium and large vesicles.

In the whole ooplasm (Table 1), mitochondria (Vv 6.5%), SER-IT (Vv 9.4%) and SER-MV (Vv 4.5%) were the organelles that occupied the highest mean relative volumes, with total SER corresponding to the highest mean relative volumes (Vv 15.05%). This was followed by aSERT (Vv 0.8%), cortical vesicles and lysosomes (Vv 0.4%), VZ vesicles (Vv 0.04%) and dictyosomes (Vv 0.01%).

By type of organelles (Table 1), cortical vesicles predominated in the oocyte cortex, but were also found in the subcortex and inner ooplasm; VZ vesicles were observed in the oocyte cortex and very rarely in the inner ooplasm; mitochondria were equally distributed with slightly higher Vv in the subcortex; dictyosomes were rare and appeared in the cortex and inner ooplasm; lysosomes were evenly distributed, with a slightly higher Vv in the inner ooplasm; aSERT were distributed regularly, with a higher Vv found in the subcortex; SER-IT were distributed regularly, with a slight progressive decrease towards the inner ooplasm; SER-SV were similarly distributed; Ser-MV were equally distributed, with a higher Vv found in the inner ooplasm; and SER-LV were found in the cortex and inner ooplasm.

In the oocyte cortex (Table 1), the most predominant organelles were SER tubules and vesicles (mainly SER-IT and SER-MV),



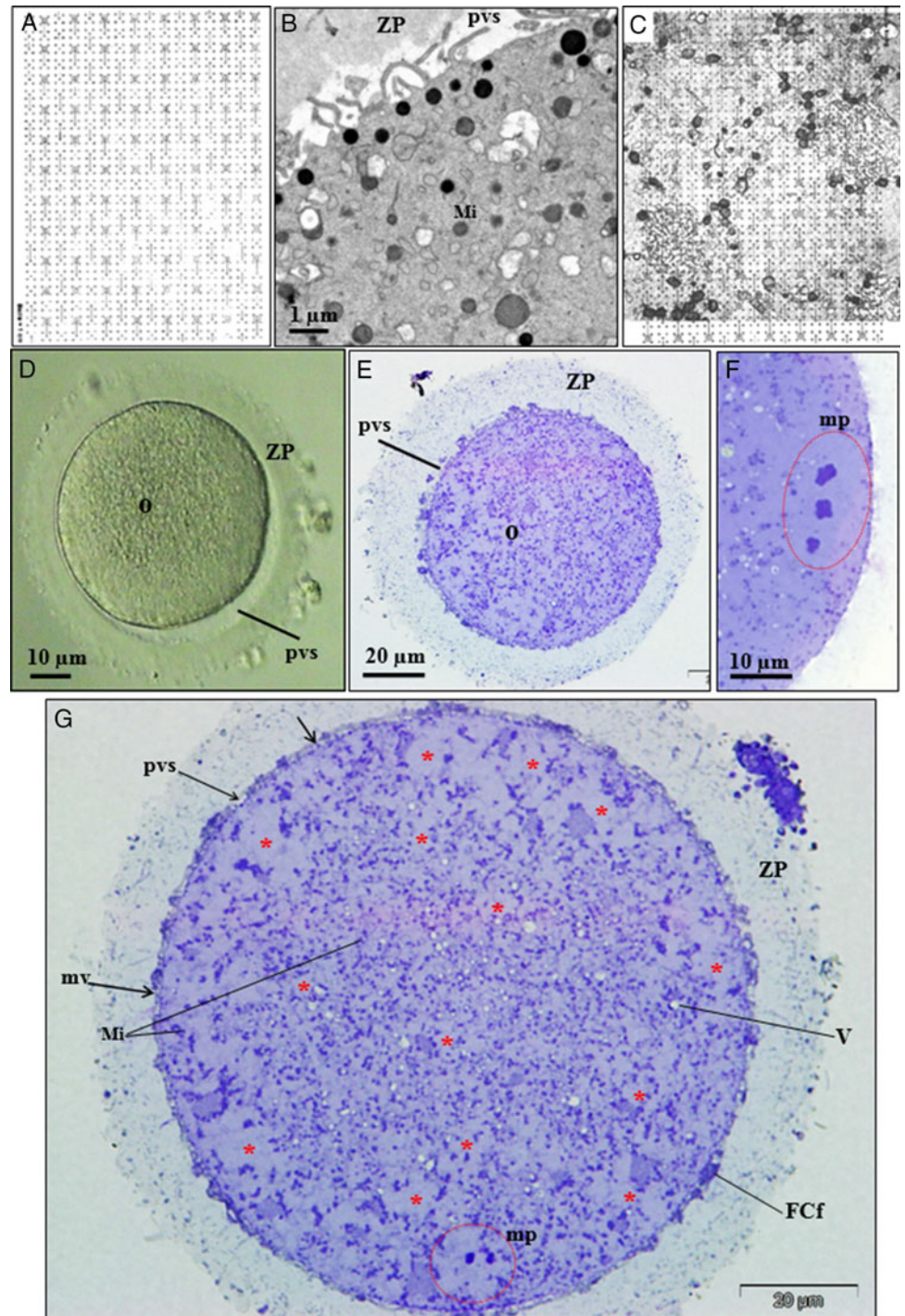


**Figure 1.** (A) Stereological grid. (B, C) Example of a micrograph region (B) with an overlapping stereological grid (C). (D) Image of a live MI oocyte observed in the inverted microscope and semithin sections of the same oocyte (E–G). The oocyte (O) appears separated from the zona pellucida (ZP) by the perivitelline space (pvs), which contains oocyte microvilli (mv) and remnants of follicular cell feet (FCf). The metaphase I plate (mp) extends from the cortex to the inner region. The oocyte cortex exhibits cortical vesicles (arrows). The ooplasm evidences mitochondria (Mi), smooth endoplasmic reticulum vesicles (V) and areas devoid of major organelles (\*).

mitochondria, aSERT and cortical vesicles. In the oocyte subcortex (Table 1), the most predominant organelles were SER tubules and vesicles (mainly SER-IT and SER-MV), mitochondria and aSERT. In the oocyte inner ooplasm (Table 1), the most predominant organelles were SER tubules and vesicles (mainly SER-IT, SER-MV and SER-LV), mitochondria and aSERT.

The three oocyte regions were compared globally using the Kruskal–Wallis test (Table 2). No significant differences were found in the mean relative volume occupied by mitochondria, dictyosomes, lysosomes, aSERT, SER-IT, and SER small and medium vesicles.

However, significant differences were observed in the mean relative volume occupied by cortical vesicles, VZ vesicles and SER-LV.

Using the Mann–Whitney *U*-test, Bonferroni-corrected, strict pairwise comparisons for the three regions were performed (Table 2). No significant differences were found between the three oocyte regions regarding the mean relative volume occupied by mitochondria, dictyosomes, lysosomes, aSERT, SER-IT, and SER small and medium vesicles. However, significant differences were observed in the mean relative volume occupied by cortical vesicles ( $V_v$  cortex >  $V_v$  subcortex,  $V_v$

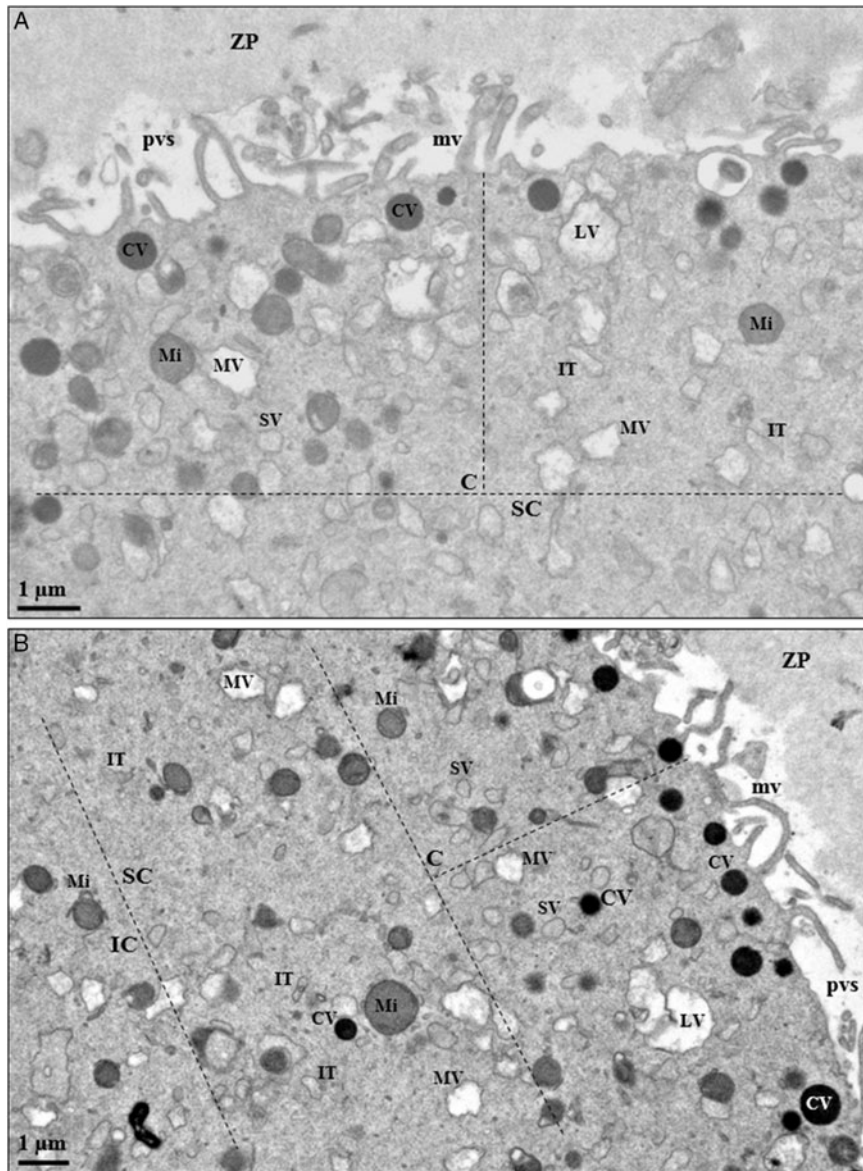


**Figure 2.** (A, B) Ultrastructural images of metaphase I oocytes showing the cortex (C), subcortex (SC) and inner (IC) oocyte regions. The distance between regions (dotted vertical lines) is of 5 µm. The distinct regions are separated by dotted transversal lines. Between the oocyte and the zona pellucida (ZP) lies the perivitelline space (pvs), which contains oocyte microvilli (mv). Cortical vesicles (CV) are mainly present in the cortex under the oolemma. Note the presence of numerous mitochondria (Mi) and smooth endoplasmic reticulum elements, including isolated tubules (IT) and small (SV) and medium (MV) vesicles. A few smooth endoplasmic reticulum large (LV) vesicles are present in the oocyte cortex.

cortex > Vv inner ooplasm), VZ vesicles (Vv cortex > Vv subcortex) and SER-LV (Vv subcortex < Vv inner ooplasm).

## Discussion

Oocyte competence is fundamental for the formation of a gamete with full embryo and implantation potential. Oocyte competence is acquired during *in vivo* maturation inside the ovarian follicle, in association with local factors, brain hormones and the surrounding follicular cells, being accomplished in an integrated mode at cytoplasmic and nuclear levels (Keef *et al.*, 2015; Conti and Franciosi, 2018; Hoshino, 2018). Regarding cytoplasmic maturation, the oocyte accumulates RNA molecules, proteins, substrates and nutrients, and calcium signalling stores (Coticchio *et al.*, 2015; Ferrer-Buitrago *et al.*, 2018). This is accompanied by the formation and spatial distribution of the major organelles, SER, mitochondria and cortical vesicles, and the cytoskeleton (Watson, 2007; Nottola *et al.*, 2014; Pires-Luis *et al.*, 2016; Sousa *et al.*, 2016; Cui and Kim, 2017; Reader *et al.*, 2017). Nuclear maturation refers to the steps involved in the resumption of meiosis, in which GV oocytes (fetal

oocytes undergo meiotic recombination and become arrested at the end of prophase I, diplotene, entering in dictyotene at birth) undergo nuclear envelope breakdown, followed by arrest at the MI stage. Under the LH surge, oocytes suffer meiosis I (chromosomal segregation with formation of the first polar body) and originate oocytes that remain arrested at the MII stage. Meiosis II (chromatid segregation with formation of the second polar body) occurs only after successful fertilization (MacLennan *et al.*, 2015; Capalbo *et al.*, 2017; Greaney *et al.*, 2018).

Numerous efforts have been developed to better understand the physiology of oocyte maturation using different 'omics approaches, such as gene expression analysis (Virant-Klun *et al.*, 2013), transcriptome studies (Labrecque and Sirard, 2014; Zhao *et al.*, 2019) and metabolomics assays (Bracewell-Milnes *et al.*, 2017). Using these techniques, upregulated and downregulated expressed genes in GV, MI and MII oocytes, mainly involved in transcription regulation, cell cycle and DNA repair pathways, were enumerated by microarray analysis (Gasca *et al.*, 2007). Single-cell proteomics identified differentially expressed proteins in GV and MI oocytes (Virant-Klun *et al.*, 2016) and DNA methylation



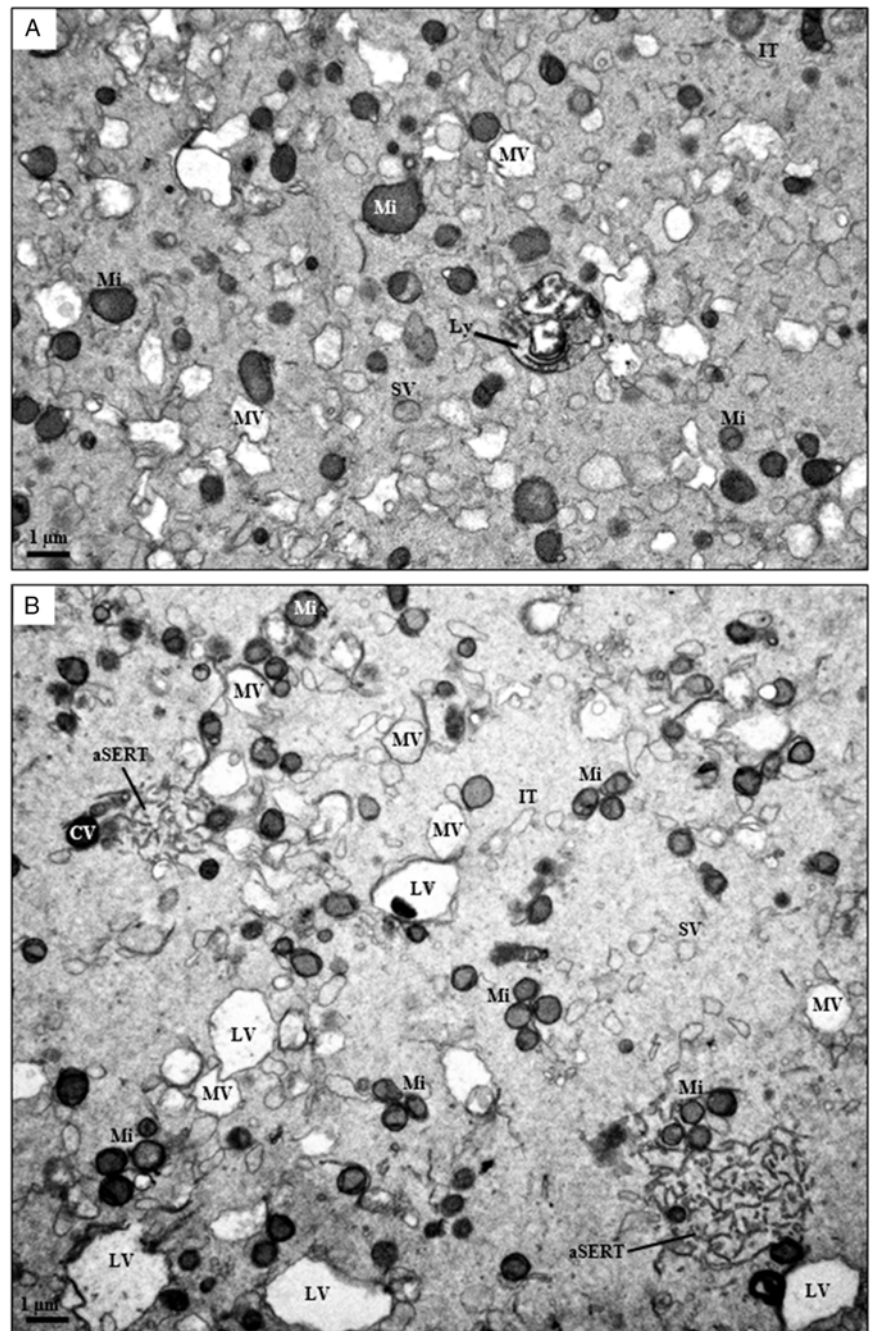


**Figure 3.** Ultrastructural images of metaphase I oocytes showing the subcortex (A) and inner (B) oocyte regions. The ooplasm evidences numerous mitochondria (Mi) and smooth endoplasmic reticulum elements, including tubular aggregates (aSERT), isolated tubules (IT) and small (SV) and medium (MV) vesicles. Smooth endoplasmic reticulum large vesicles (LV) were observed only in the inner ooplasm. In these sections, one lysosome (Ly) and a cortical vesicle (CV) can also be observed.

patterns were determined by single-cell whole genome analysis in GV, MI and MII oocytes (Yu *et al.*, 2017).

Several mechanisms for MI arrest have been raised. Some authors have suggested that the MI arrest could be due to an incomplete or absent LH effect, to disturbances in signalling mechanisms between oocyte and cumulus cells, or intrinsic oocyte factors (Coticchio *et al.*, 2015). Of the intrinsic factors, the authors suggested that MI arrest could be due to loss of the meiotic checkpoint, in which the maturation-promoting factor (MPF), a metaphase (M-phase)-specific kinase would remain inactive or that MI arrest could be due to abnormal spindle formation (Mehlmann, 2005; Madgwick and Jones, 2007). Other authors have suggested four major mechanisms, cytoplasmic

incompetence, disruption of factors involved in meiotic recombination, loss of MPF activation and cytoskeleton anomalies (Mrazek and Fulka, 2003; Mehlmann, 2005; Madgwick and Jones, 2007; Coticchio *et al.*, 2015). Other authors offered a sustained review of all cases and results with animal models. This analysis revealed that, of all the factors presented above, the main cause of MI arrest would be due to signal transduction pathways that mediate meiotic progression or abnormalities in the meiotic spindle (Beall *et al.*, 2010). More recently, MI arrest has been related to spindle assembly checkpoint defects (Tripathi *et al.*, 2010; Marangos *et al.*, 2015; Liu *et al.*, 2016), *TUBB8* tubulin gene mutations, whose expressed protein is a member of the meiotic spindle microtubules (Feng *et al.*, 2016; Chen *et al.*, 2017a) and with mutations in the

**Table 1.** Relative volume of organelles (Vv) per MI oocyte, oocyte cortex, subcortex and inner cytoplasm

Organelle	Vv (organelle, oocyte) Mean (%) ± SEM (CVar)	Vv (organelle, cortex) Mean (%) ± SEM (CVar)	Vv (organelle, subcortex) Mean (%) ± SEM (CVar)	Vv (organelle, inner cytoplasm) Mean (%) ± SEM (CVar)
CV	0.4 ± 0.07 (0.42)	0.96 ± 0.17 (0.39)	0.1 ± 0.03 (0.49)	0.1 ± 0.03 (0.82)
VZ	0.04 ± 0.03 (1.49)	0.1 ± 0.07 (1.58)	0	0.01 ± 0.005 (1.67)
Mi	6.5 ± 0.59 (0.20)	6.3 ± 0.23 (0.08)	7.3 ± 0.39 (0.12)	6.4 ± 0.86 (0.30)
Di	0.01 ± 0.004 (0.91)	0.01 ± 0.01 (1.63)	0	0.01 ± 0.006 (1.28)
Ly	0.4 ± 0.09 (0.57)	0.3 ± 0.08 (0.71)	0.3 ± 0.13 (0.95)	0.4 ± 0.11 (0.57)
aSERT	0.8 ± 0.25 (0.69)	1.02 ± 0.33 (0.72)	1.3 ± 0.46 (0.80)	0.6 ± 0.22 (0.86)
SER-IT	9.4 ± 0.50 (0.12)	10.4 ± 0.42 (0.09)	9.6 ± 0.46 (0.11)	8.8 ± 0.59 (0.15)
SER-SV	0.2 ± 0.06 (0.68)	0.2 ± 0.07 (0.73)	0.2 ± 0.08 (0.79)	0.2 ± 0.06 (0.68)
SER-MV	4.5 ± 1.003 (0.50)	4.1 ± 1.18 (0.64)	3.5 ± 1.02 (0.64)	4.7 ± 0.96 (0.45)
SER-LV	0.2 ± 0.06 (0.91)	0.07 ± 0.03 (1.05)	0	0.2 ± 0.1 (1.02)
Total SER (SV, MV, LV, IT, aSERT)	15.05 ± 1.25 (0.19)	15.9 ± 1.27 (0.18)	14.6 ± 1.35 (0.21)	14.5 ± 1.38 (0.21)

Results presented as mean (%), SEM: standard error of the mean (standard deviation/ $n^{1/2}$ ), and CVar: coefficient of variation (standard deviation/mean).

CV: cortical vesicles; VZ: vesicles with granular material; Mi: mitochondria; Di: dictyosomes; Ly: lysosomes; SER: smooth endoplasmic reticulum; aSERT: SER tubular aggregates; SER-IT: SER tubules; SER-SV: SER small vesicles; SER-MV: SER medium vesicles; SER-LV: SER large vesicles.

**Table 2.** Comparison of the means of Vv (organelle, cortex), Vv (organelle, subcortex) and Vv (organelle, inner cytoplasm) in MI oocytes

Organelle	Kruskal–Wallis test ( <i>P</i> -value*)	Oocyte regions	Mann–Whitney test ( <i>P</i> -value*)
CV	0.004	Cortex vs Subcortex (Vv 0.96 vs Vv 0.1)	0.008
		Cortex vs. Inner Cytoplasm (Vv 0.96 vs Vv 0.1)	0.008
VZ	0.005	Cortex vs. Subcortex (Vv 0.1 vs Vv 0)	0.008
Mi	0.432		
Di	0.182		
Ly	0.754		
aSERT	0.468		
SER-IT	0.061		
SER-SV	0.811		
SER-MV	0.403		
SER-LV	0.011	Subcortex vs Inner Cytoplasm (Vv 0 vs Vv 0.2)	0.008
Total SER	0.756		

\*Significance set at  $P < 0.05$ .

CV: cortical vesicles; VZ: vesicles with granular materials; Mi: mitochondria; Di: dictyosomes; Ly: lysosomes; SER: smooth endoplasmic reticulum; aSERT: SER tubular aggregates; SER-IT: SER tubules; SER-SV: SER small vesicles; SER-MV: SER medium vesicles; SER-LV: SER large vesicles.

*PATL2* gene, whose protein is related to topoisomerase II, a critical enzyme involved in DNA replication, including meiosis (Chen *et al.*, 2017b).

There are no ultrastructural studies dedicated exclusively to human MI oocytes. Of the works giving data substantiated by images, we found similar findings regarding the type of perivitelline space (narrow), microvilli (numerous, narrow and long),

mitochondria, and SER vesicles and tubules (Zamboni *et al.*, 1972; Sundström *et al.*, 1985a,b; El Shafie *et al.*, 2000; Sathanathan, 2000, 2003); presence of aSERT (Zamboni *et al.*, 1972; Sundström *et al.*, 1985a,b); distribution of cortical vesicles forming one or two rows (Zamboni *et al.*, 1972; Sundström *et al.*, 1985a,b; El Shafie *et al.*, 2000; Sathanathan, 2000, 2003); secondary lysosomes with heterogeneous contents (Sundström *et al.*, 1985a,b; El Shafie *et al.*, 2000; Sathanathan, 2003); presence of coated-vesicles (Sathanathan, 2003); and presence of areas devoid of organelles (Sundström *et al.*, 1985a; Motta *et al.*, 1988). In accordance with those previous studies, we did not find multivesicular bodies, annulate lamellae, rough endoplasmic reticulum, polyribosomes or lipid droplets.

Although ultrastructural observations can describe in detail the morphology of oocyte components, they are unable to provide reliable information on the actual distribution of organelles. To overcome this limitation, we here presented a stereological analysis of human MI oocytes, providing the mean relative volumes occupied by each organelle and their relative positions. Total SER vesicles and tubules (Vv 15.05%) and mitochondria (Vv 6.5%) were the organelles that occupied the highest mean relative volumes. These were evenly distributed across all oocyte regions. Of the SER components, SER tubules (9.4%) and SER-MV (4.5%) presented the highest mean relative volumes and were also evenly distributed, while aSERT predominated in the oocyte sub-cortex and cortex, SER-SV appeared uniformly distributed and SER-LV predominated in the inner ooplasm. Dictyosomes were rare and small, being found in the cortex and inner ooplasm. Lysosomes with heterogeneous materials were frequent and lacked precise location. They reflect an active metabolism and autophagy in the immature MI oocyte. Cortical vesicles were predominantly observed under the oolemma and, as expected in an immature oocyte, isolated cortical vesicles were still observed in the subcortex and inner ooplasm. Granular content vesicles were observed in the oocyte cortex. These vesicles apparently fused with the oolemma, releasing their contents into the perivitelline space, reaching the inner ZP. Similar vesicles were observed in human GV oocytes,

**Table 3.** Comparison of the means of Vv (organelle, cortex-c), Vv (organelle, subcortex-sc) and Vv (organelle, inner cytoplasm-ic) between GV oocytes and MI oocytes

Organelle	Vv (organelle, oocyte) GV vs MI GV ( <i>P</i> -value)*, MI**	Vv (organelle, c) GV vs MI GV ( <i>P</i> -value) MI	Vv (organelle, sc) GV vs MI GV ( <i>P</i> -value) MI	Vv (organelle, ic) GV vs MI GV ( <i>P</i> -value) MI
CV (Vv)	0.3 (0.612) 0.4	1.3 (0.268) 0.96	0.1 (0.530) 0.1	0.1 (0.432) 0.1
Mi (Vv)	6.3 (0.089) 6.5	3.6 (0.01) 6.3	6.0 (0.073) 7.3	7.2 (0.530) 6.4
Di (Vv)	0.5 (<0.001) 0.01	0.4 (0.003) 0.01	0.6 (0.010) 0	0.6 (0.003) 0.01
Ly (Vv)	0.2 (0.067) 0.4	0.1 (0.202) 0.3	0.1 (0.432) 0.3	0.3 (0.639) 0.4
SER-IT (Vv)	3.2 (<0.001) 9.4	3.3 (0.005) 10.4	3.2 (0.003) 9.6	3.1 (0.003) 8.8
SER-SV (Vv)	2.5 (<0.001) 0.2	2.0 (0.003) 0.2	2.3 (0.003) 0.2	2.7 (0.003) 0.2
SER-MV (Vv)	0.2 (<0.001) 4.5	0.1 (0.003) 4.1	0.2 (0.003) 3.5	0.3 (0.003) 4.7
SER-LV (Vv)	0.2 (0.072) 0.2	0.07 (0.876) 0.07	0.1 (0.010) 0	0.2 (0.876) 0.2
Total SER (Vv)	6.1 (<0.001) 15.05	4.6 (0.003) 15.9	5.8 (0.003) 14.6	6.23 (0.003) 14.5

\*Significance set at  $P < 0.05$

\*\*Data are presented as the Vv found in the different organelles in GV oocytes (from Pires-Luís *et al.*, 2016), the comparative *P*-value between the Vv of GV vs MI oocytes for each organelle, and the Vv found in the different organelles in MI oocytes (from Table 1). GV: prophase I oocytes (germinal vesicle stage); MI: metaphase-I oocytes; CV: cortical vesicles; Mi: mitochondria; Di: dictyosomes; Ly: lysosomes; SER: smooth endoplasmic reticulum; aSERT: SER tubular aggregates; SER-IT: SER tubules; SER-SV: SER small vesicles; SER-MV: SER medium vesicles; SER-LV: SER large vesicles.

in which they were suggested to deliver zona pellucida-like components to the extracellular milieu (Pires-Luís *et al.*, 2016). The oocyte submembranar region presented tiny coated-vesicles, suggesting active receptor-mediated endocytosis, which reinforces that the immature MI oocyte remains active in absorption of elements from the external milieu. The MI oocyte cytoplasm evidenced a network of areas devoid of major organelles, larger in the subcortex oocyte region. Future work is needed as these regions may represent a stock of molecules or energy constituents for current use and ready to use after fertilization.

We previously quantified by stereological methods the mean relative volumes occupied by each organelle and their relative distribution in human GV oocytes (Pires-Luís *et al.*, 2016). Regarding morphology, MI oocytes as GV oocytes did not present rough endoplasmic reticulum, lipid droplets and polyribosomes. In opposite, MI oocytes did not present LV containing zona-pellucida-like materials, multivesicular bodies, annulate lamellae and SER very LV (SER-VLV), and GV oocytes did not present VZ vesicles, aSERT or associations between mitochondria and SER elements. Regarding the total mean relative volumes, GV oocytes displayed a predominance of SER-VLV (mainly in the inner ooplasm), mitochondria and total SER elements (Pires-Luís *et al.*, 2016). MI oocytes also revealed a predominance of mitochondria and total SER, but instead of SER-VLV, which does not exist in MI oocytes, this predominance was replaced by SER-MV.

Comparative quantitative data between MI and GV oocytes using strict pairwise comparisons for the three oocyte regions (Table 3) revealed several other differences between them. Both MI and GV oocytes exhibited a prevalence of cortical vesicles in the oocyte cortex. In MI oocytes, mitochondria were evenly distributed, with significant differences to GV oocytes observed only at the cortex (higher in MI), while in GV oocytes mitochondria predominated in the inner regions. There were no significant differences between MI and GV oocytes regarding regular lysosome distribution. In all oocyte regions, there were significant lower mean relative volumes of dictyosomes and SER-SV and significant higher mean relative volumes of SER-MV, SER-IT and total SER elements, in MI oocytes. When the three oocyte regions were compared globally, significant differences were observed in the mean relative volume occupied by dictyosomes (higher

in GV), SER-IT (higher in MI), SER-SV (higher in GV), SER-MV (higher in MI) and total SER (higher in MI).

Despite thorough quantitative assessments, the main limitation of the present study is the limited number of MI oocytes evaluated (five). This limitation was imposed by the low availability of MI oocytes at our IVF facilities. However, it should be noted that the oocytes used in this study were retrieved from five different women, which allowed a more heterogeneous sample.

In conclusion, we present here a stereological quantitative evaluation of human MI oocytes. The data revealed a homogeneous organelle distribution (mitochondria, dictyosomes, lysosomes and SER), except for the predominance of cortical vesicles and VZ vesicles in the oocyte cortex and SER-LV in the inner cytoplasm. The MI oocyte was extremely rich in mitochondria, SER medium vesicles and tubules. The MI oocyte already presented well-developed SER tubular aggregates associated with mitochondria, which in the mature MII oocyte are known to actively participate in calcium signalling at fertilization (Sousa *et al.*, 1996, 1997). Additionally, the MI oocyte cortex still evidences signs of ZP material export from the oocyte and active endocytosis.

**Supplementary material.** To view supplementary material for this article, please visit <https://doi.org/10.1017/S0967199420000131>

**Financial Support.** This research did receive no grants from funding commercial agencies. UMIB (Pest-OE/SAU/UI0215/2014) is funded by National Funds through FCT-Foundation for Science and Technology.

**Conflicts of interest.** The authors declare to have no competing interests.

**Compliance with ethical standards.** The authors declare that they have followed all rules of ethical conduct regarding originality, data processing and analysis, duplicate publication and biological material.

## References

- Álvarez C, García-Garrido C, Taronger R and González de Merlo G (2013) *In vitro* maturation, fertilization, embryo development and clinical outcome of human metaphase-I oocytes retrieved from stimulated intracytoplasmic sperm injection cycles. *Indian J Med Res* **137**, 331–8.
- Beall S, Brenner C and Segars J (2010) Oocyte maturation failure: a syndrome of bad eggs. *Fertil Steril* **94**, 2507–13.



- Bracewell-Milnes T, Saso S, Abdalla H, Nikolau D, Norman-Taylor J, Johnson M, Holmes E and Thum M-Y (2017) Metabolomics as a tool to identify biomarkers to predict and improve outcomes in reproductive medicine: a systematic review. *Hum Reprod Update* **23**, 723–36.
- Capalbo A, Hoffmann ER, Cimadomo D, Ubaldi FM and Rienzi L (2017) Human female meiosis revised: new insights into the mechanisms of chromosome segregation and aneuploidies from advanced genomics and time-lapse imaging. *Hum Reprod Update* **23**, 706–22.
- Cha K-Y and Chian R-C (1998) Maturation *in vitro* of immature human oocytes for clinical use. *Hum Reprod Update* **4**, 103–20.
- Chen B, Li B, Li D, Yan Z, Mao X, Xu Y, Mu J, Li Q, Jin L, He L, Kuang Y, Sang Q and Wang L (2017a) Novel mutations and structural deletions in *TUBB8*: expanding mutational and phenotypic spectrum of patients with arrest in oocyte maturation, fertilization or early embryonic development. *Hum Reprod* **32**, 457–64.
- Chen B, Zhang Z, Sun X, Kuang Y, Mao X, Wang X, Yan Z, Li B, Xu Y, Yu M, Fu J, Mu J, Zhou Z, Li Q, Jin L, He L, Sang Q and Wang L (2017b) Biallelic mutations in *PATL2* cause female infertility characterized by oocyte maturation arrest. *Am J Hum Genet* **101**, 609–15.
- Chian R-C, Uzelac PS and Nargund G (2013) *In vitro* maturation of human immature oocytes for fertility preservation. *Fertil Steril* **99**, 1173–81.
- Conti M and Franciosi F (2018) Acquisition of oocyte competence to develop as an embryo: integrated nuclear and cytoplasmic events. *Hum Reprod Update* **24**, 245–66.
- Coticchio G, Dal Canto M, Renzini MM, Guglielmo MC, Brambillasca F, Turchi D, Novara PV and Fadini R (2015) Oocyte maturation: gamete-somatic cell interactions, meiotic resumption, cytoskeletal dynamics and cytoplasmic reorganization. *Hum Reprod Update* **21**, 427–54.
- Cui X-S and Kim N-H (2017) Maternally derived transcripts: identification and characterization during oocyte maturation and early cleavage. *Reprod Fertil Dev* **19**, 25–34.
- El Shafie M, Windt M-L, Kitshoff M, McGregor P, Sousa M, Wrang PAB and Kruger TF (2000) Ultrastructure of human oocytes: a transmission electron microscopy view. In *An Atlas of the Ultrastructure of Human Oocytes* (eds M El Shafie, M Sousa, M-L Windt and TF Kruger), pp. 83–173. The Parthenon Publishing Group.
- Familiari G, Makabe S and Motta PM (1989) The ovary and ovulation: a three dimensional ultrastructural study. In *Ultrastructure of Human Gametogenesis and Early Embryogenesis* (eds JV Blerkom and PM Motta), pp. 85–124. Kluwer Academic Publishers, Boston, MA, USA.
- Feng R, Sang Q, Kuang Y, Sun X, Yan Z, Zhang S, Shi J, Tian G, Luchniak A, Fukuda Y, Li B, Yu M, Chen J, Xu Y, Guo L, Qu R, Wang X, Sun Z, Liu M, Shi H, Wang H, Feng Yi, Shao R, Chai R, Li Q, Xing Q, Zhang R, Nogales E, Jin L, He L, Gupta Jr ML, Cowan NJ and Wang L (2016) Mutations in *TUBB8* cause human oocyte meiotic arrest. *N Engl J Med* **374**, 223–32.
- Ferrer-Buitrago M, Dhaenens L, Lu Y, Bonte D, Vanden Meerschaut F, De Sutter P, Leybaert L and Heindryckx B (2018) Human oocyte calcium analysis predicts the response to assisted oocyte activation in patients experiencing fertilization failure after ICSI. *Hum Reprod* **33**, 416–25.
- Gasca S, Pellestor F, Assou S, Loup V, Anahory T, Dechaud H, De Vos J and Hamamah S (2007) Identifying new human oocyte marker genes: a microarray approach. *Reprod Biomed Online* **14**, 175–83.
- Greaney J, Wei Z and Homer H (2018) Regulation of chromosome segregation in oocytes and the cellular basis for female meiotic errors. *Hum Reprod Update* **24**, 135–61.
- Hoshino Y (2018) Updating the markers for oocyte quality evaluation: intracellular temperature as a new index. *Reprod Med Biol* **17**, 434–41.
- Huirne JA, Homburg R and Lambalk CB (2007) Are GnRH antagonists comparable to agonists for use in IVF? *Hum Reprod* **22**, 2805–13.
- Keef D, Kumar M and Kalmbach K (2015) Oocyte competency is the key to embryo potential. *Fertil Steril* **103**, 317–22.
- Labrecque R and Sirard M-A (2014) The study of mammalian oocyte competence by transcriptome analysis: progress and challenges. *Mol Hum Reprod* **20**, 103–16.
- Levrin D, Farhi J, Nahum H, Glezerman M and Weissman A (2002) Maturation arrest of human oocytes as a cause of infertility. *Hum Reprod* **17**, 1604–9.
- Li Y, Liu H, Yu Q, Liu H, Huang T, Zhao S, Ma J and Zhao H (2019) Growth hormone promotes *in vitro* maturation of human oocytes. *Front Endocrinol* **10**, 485.
- Liu C, Li M, Li T, Zhao H, Huang J, Wang Y, Gao Q, Yu Y and Shi Q (2016) ECATI is essential for human oocyte maturation and pre-implantation development of the resulting embryos. *Sci Rep* **6**, 38192.
- MacLennan M, Crichton JH, Playfoot CJ and Adams IR (2015) Oocyte development, meiosis and aneuploidy. *Semin Cell Dev Biol* **45**, 68–76.
- Madgwick S and Jones KT (2007) How eggs arrest at metaphase II: MPF stabilization plus APC/C inhibition equals cytostatic factor. *Cell Division* **2**, 4.
- Marangos P, Stevense M, Niaka K, Lagoudaki M, Nabti I, Jessberger R and Carroll J (2015) DNA damage-induced metaphase I arrest is mediated by the spindle assembly checkpoint and maternal age. *Nat Commun* **6**, 8706.
- Mehlmann LM (2005) Stops and starts in mammalian oocytes: recent advances in understanding the regulation of meiotic arrest and oocyte maturation. *Reproduction* **130**, 791–9.
- Morimoto Y (2009) Ultrastructure of the human oocytes during *in vitro* maturation. *J Mamm Ova Res* **26**, 10–7.
- Motta PM, Nottola SA, Micara G and Familiari G (1988) Ultrastructure of human unfertilized oocytes and polyspermic embryos in an IVF-ET program. *Ann NY Acad Sci* **541**, 367–83.
- Mrazek M and Fulka Jr J (2003) Failure of oocyte maturation: possible mechanism for oocyte maturation arrest. *Hum Reprod* **18**, 2249–52.
- Nogueira D, Romero S, Vanhoutte L, de Matos DG and Smitz J (2009) Oocyte *in vitro* maturation. In *Textbook of Assisted Reproductive Technologies* 3rd edn (eds DK Gardner, A Weissman, CM Howles and Z Shoham) pp. 111–153. London UK: Informa Healthcare.
- Nottola SA, Macchiarelli G and Familiari G (2014) Fine structural markers of human oocyte quality in assisted reproduction. *Austin J Reprod Med Infertil* **1**, 5.
- Pinto F, Oliveira C, Cardoso MF, Teixeira da Silva J, Silva J, Sousa M and Barros A (2009) Impact of GnRH ovarian stimulation protocols on intracytoplasmic sperm injection outcomes. *Reprod Biol Endocrinol* **7**, 5.
- Pires-Luis AS, Rocha E, Bartosch C, Oliveira E, Silva J, Barros A, Sá R and Sousa M (2016) A stereological study on organelle distribution in human oocytes at prophase I. *Zygote* **24**, 346–54.
- Reader KL, Stanton J-AL and Juengel J (2017) The role of oocyte organelles in determining developmental competence. *Biology* **6**, 35.
- Richani D and Gilchrist RB (2018) The epidermal growth factor network: role in oocyte growth, maturation and developmental competence. *Hum Reprod Update* **24**, 1–14.
- Sá R, Cunha M, Silva J, Luís A, Oliveira C, Teixeira da Silva J, Barros A and Sousa M (2011) Ultrastructure of tubular smooth endoplasmic reticulum aggregates in human metaphase II oocytes and clinical implications. *Fertil Steril* **96**, 143–9.
- Sathananthan AH (1985) Maturation of the human oocyte *in vitro*: nuclear events during meiosis (an ultrastructural study). *Gamete Res* **12**, 237–54.
- Sathananthan AH (1994) Ultrastructural changes during meiotic maturation in mammalian oocytes: unique aspects of the human oocyte. *Microsc Res Tech* **27**, 145–64.
- Sathananthan AH (2000) Ultrastructure of human gametes, fertilization, and embryo development. In *Handbook of In Vitro Fertilization* 2nd edn (eds AO Trouson and DK Gardner), pp. 431–64. Boca Raton, FL, USA: CRC Press LLC.
- Sathananthan AH (2003) Morphology and pathology of the human oocyte. In *Biology and Pathology of the Oocyte* 1st edn (eds AO Trouson and RG Gosden), pp. 185–208. Cambridge, UK: Cambridge University Press.
- Sathananthan AH, Trouson AO and Wood C (1986) Oocyte maturation. In *Atlas of Fine Structure of Human Sperm Penetration, Eggs and Embryos Cultured In Vitro* (eds AH Sathananthan, AO Trouson and C Wood), pp. 1–47. New York, USA: Praeger Publishers.
- Smitz JEJ, Thompson JG and Gilchrist RB (2011) The promise of *in vitro* maturation in assisted reproduction and fertility preservation. *Semin Reprod Med* **29**, 24–37.
- Sousa M and Tesarik J (1994) Ultrastructural analysis of fertilization failure after intracytoplasmic sperm injection. *Hum Reprod* **9**, 2374–80.

- Sousa M, Barros A and Tesarik J** (1996) Developmental changes in calcium dynamics, protein kinase C distribution and endoplasmic reticulum organization in human preimplantation embryos. *Mol Hum Reprod* **2**, 967–77.
- Sousa M, Barros A, Silva J and Tesarik J** (1997) Developmental changes in calcium content of ultrastructurally distinct subcellular compartments of preimplantation human embryos. *Mol Hum Reprod* **3**, 83–90.
- Sousa M, Oliveira E, Barros N, Barros A and Sá R** (2016) New ultrastructural observations of human oocyte smooth endoplasmic reticulum tubular aggregates and cortical reaction: update on the molecular mechanisms involved. *Rev Int Androl* **14**, 113–22.
- Strassburger D, Friedler S, Raziel A, Kasterstein E, Schachter M and Ron-El R** (2004) The outcome of ICSI of immature MI oocytes and rescued *in vitro* matured MII oocytes. *Hum Reprod* **19**, 1587–90.
- Strassburger D, Goldstein A, Friedler S, Raziel A, Kasterstein E, Mashevich M, Schachter M, Ron-El R and Reish O** (2010) The cytogenic constitution of embryos derived from immature (metaphase I) oocytes obtained after ovarian hyperstimulation. *Fertil Steril* **94**, 971–8.
- Sundström P and Nilsson BO** (1988) Meiotic and cytoplasmic maturation of oocytes collected in stimulated cycles is asynchronous. *Hum Reprod* **3**, 613–9.
- Sundström P, Nilsson BO, Liedholm P and Larsson E** (1985a) Ultrastructural characteristics of human oocytes fixed at follicular puncture or after culture. *J In Vitro Fert Embryo Transf* **2**, 195–206.
- Sundström P, Nilsson BO, Liedholm P and Larsson E** (1985b) Ultrastructure of maturing human oocytes. *Ann NY Acad Sci* **442**, 324–31.
- Tripathi A, Kumar P and Chaube SK** (2010) Meiotic cell cycle arrest in mammalian oocytes. *J Cell Physiol* **223**, 592–600.
- Vanhoutte L, De Sutter P, Van der Elst J and Dhont M** (2005) Clinical benefit of metaphase I oocytes. *Reprod Biol Endocrinol* **3**, 71.
- Virant-Klun I, Knez K, Tomazevic T and Skutella T** (2013) Gene expression profiling of human oocytes developed and matured *in vivo* or *in vitro*. *Biomed Res Int* 2013, Article ID 879489.
- Virant-Klun I, Leicht S, Hughes C and Krijgsveld J** (2016) Identification of maturation-specific proteins by single-cell proteomics of human oocytes. *Mol Cell Proteomics* **15**, 2616–27.
- Watson AJ** (2007) Oocyte cytoplasmic maturation: a key mediator of oocyte and embryo developmental competence. *J Anim Sci* **85**, E1–3.
- Weibel ER, Kistler GS and Scherle WF** (1966) Practical stereological methods for morphometric cytology. *J Cell Biol* **30**, 23–38.
- Windt M-L, Coetzee K, Kruger TF, Marino H, Kitshoff MS and Sousa M** (2001) Ultrastructural evaluation of recurrent and *in vitro* maturation resistant metaphase I arrested oocytes. *Hum Reprod* **16**, 2394–8.
- Yu B, Dong X, Gravina S, Kartal Ö, Schimmel T, Cohen J, Tortoriello D, Zody R, Hawkins RD and Vijg J** (2017) Genome-wide, single-cell DNA methylomics reveals increased non-CpG methylation during human oocyte maturation. *Stem Cell Rep* **9**, 397–407.
- Zamboni L, Thompson RS and Smith DM** (1972) Fine morphology of human oocyte maturation *in vitro*. *Biol Reprod* **7**, 425–57.
- Zhao H, Li T, Yue Zhao, Tan T, Liu C, Liu Y, Chang L, Huang N, Li C, Fan Y, Yu Y, Li R and Qiao J** (2019) Single-cell transcriptomics of human oocytes: environment-driven metabolic competition and compensatory mechanisms during oocyte maturation. *Antioxid Redox Signal* **30**, 542–59.